Arabian Journal of Chemistry (2020) **13**, 8411–8423

King Saud University

Arabian Journal of Chemistry

www.ksu.edu.sa
www.sciencedirect.com

ORIGINAL ARTICLE

Biosynthesis and characterization of lead selenide semiconductor nanoparticles (PbSe NPs) and its antioxidant and photocatalytic activity

Catherine Sekyerebea Diko, Yuanyuan Qu *, Zhang Henglin, Zheng Li, Noor Ahmed Nahyoon, Shuling Fan

State Key Laboratory of Industrial Ecology and Environmental Engineering (Ministry of Education), School of Environmental Science and Technology, Dalian University of Technology, Dalian 116024, China

Received 28 February 2020; accepted 3 June 2020
Available online 17 June 2020

KEYWORDS

Lead selenide nanoparticles;
Trichoderma sp. WL-Go;
Antioxidant activity;
Photocatalyst;
Rhodamine B

Abstract The current study fabricated novel lead selenide nanoparticles (PbSe NPs) by a simple biological benign process with *Trichoderma* sp. WL-Go. Ultraviolet–visible spectroscopy (UV–vis), Transmission electron microscopy (TEM), X-ray diffraction (XRD), Fourier transfer infrared (FTIR) spectroscopic analysis, Raman spectroscopy and Photoluminescence (PL) were used to characterize the physicochemical properties of the fabricated NPs. Synthesis at pH 8 with 0.5 g biomass of strain WL-Go and (1:1) mM of SeO_2: $Pb(NO_3)_2$ were the optimal synthesis conditions to achieving 10–30 nm cubic faced centered NPs. The PbSe NPs served as catalyst for investigating the antioxidant activity using 2,2-diphenyl-1-picrylhydrazyl (DPPH) and photodegradation ability of rhodamine B dye (10 mg/L). The results indicated that the NPs could eliminate up to 88.60% of free radicals after adding 600 g/mL NPs and could photodegrade 82% of rhodamine B in 30 min. Thus, this study provides new knowledge and strategies for the future use of an environmentally benign bio- catalytic PbSe NPs to efficiently eliminate free radicals and in treatment of persistent organic pollutants in wastewaters.

1. Introduction

There are rising interests in the synthesis of nanomaterials owing to their potential applications in various fields like catalysis, electronic, magnetic etc. (Panda et al., 2018; Xu and Lee, 2014; Kumar et al., 2017). In the synthesis of nanoparticles, there are two alternatives approaches to consider. The "top-down" approach where materials are reduced in size using physical or chemical means and "bottom-up" approach using chemical or biological procedure(s) for synthesis (Thakkar

* Corresponding author.
E-mail address: qyy@dlut.edu.cn (Y. Qu).
Peer review under responsibility of King Saud University.

Production and hosting by Elsevier

https://doi.org/10.1016/j.arabjc.2020.06.005
1878-5352 © 2020 Published by Elsevier B.V. on behalf of King Saud University.

et al., 2010). The bottom-up technique offers the power of manipulating the atomic or molecular levels given rise to structures of desired geometry and properties thereby reducing the use of industrial chemicals (Sharma et al., 2019). The structures of semiconductor nanoparticles exhibit distribution patterns of the two elements either oriented randomly with an intermetallic compound, cluster-in-cluster or core-shell alloy structures (Zaleska-Medynska et al., 2016; Yang et al., 2008; Paszkiewicz et al., 2016). The preparation methods, synthesis conditions and physicochemical properties of the precursors determine the orientation, shape and size of the final synthesized nanoparticles and their applications (Ali et al., 2016; Kolahalam et al., 2019).

Lead selenide (PbSe) has a narrow-band gap of 0.27 eV (Krishna et al., 2018; Ren et al., 2018; Sun et al., 2015), furthermore, it is classified as a direct semiconductor in which the momentum of electrons and holes is the same in both the conduction and valence bands. This leads to the fast recombination of produced electron-hole pairs (Khataee et al., 2015b). PbSe is a member of the IV–VI group with a cubic NaCl-like structure (Anwar et al., 2015). Also, it has wide application in thermoelectric materials and can be potentially used as an effective and promising visible light-driven photocatalyst for water and wastewater treatment (Khataee et al., 2015a, 2015b; Qu et al., 2013).

Fungi have been widely used in the synthesis of nanoparticles owing to their ease in handling, high growth rate and biomass production, secretion of large quantities of metabolic enzymes and extracellular proteins which act as reducing and capping agent in nanoparticles production (Guilger-Casagrande et al., 2019). *Trichoderma* species are further are rich in redox proteins, polysaccharides, exhibit better stability and are easy to separate in its applications (Horta et al., 2018). Exposure of fungal mycelium to precursors trigger the fungus to produce enzymes and metabolites that act as detoxifiers for the organism and in turn transforms the precursors into noble synthesized nanoparticles (Jacob et al., 2017; Vahabi et al., 2011). Hence, the detoxifying mechanism results in the reduction and capping of the NPs given rise to greater colloidal stability with respect to factors like pH, growth time, temperature, etc. used in synthesis (Rajput et al., 2016; Rajendran and Sen, 2016). *Trichoderma* sp. WL-Go (KM242362.1) was firstly isolated from activated sludge samples of an antibiotic-contaminated bioreactor (Dalian, China) and the strain colonies showed green concentric round striate on agar plate (Qu et al., 2017). This fungus strain after isolation was further used to synthesize gold nanoparticles and exhibited remarkable photocatalytic decolorization degradation against various azo dyes and the catalytic degradation of aromatic pollutants(Qu et al., 2018). These properties and characteristics make *Trichoderma* sp. WL-Go viable in the synthesis of semiconductor NPs.

Biologically synthesized semiconductor nanoparticles have been shown to have enhanced selectivity and improved stability with developed fundamental structures (Malarkodi et al., 2014). This is due to the surface interaction between the reducing agents and precursors (Han et al., 2019). Hence, synthesis of semiconductor nanoparticles with controlled size, morphology and composition are of immense interest due to their distinctive physical and chemical properties as compared to their bulk counterparts (Syed and Ahmad, 2013; Alruqi et al., 2019). The fungus *Fusarium oxysporum* (Syed and Ahmad, 2013), *Klebsiella pneumonia* (Malarkodi et al., 2014), *Serratia nematodiphila* (Malarkodi et al., 2013) have been reported to fabricate semiconductor nanoparticles. Several literatures have reported on the synthesis of PbSe NPs but majority of them are chemically synthesized (Gervas et al., 2016; Sankapal et al., 2011). In terms of biological synthesis of PbSe NPs, just a hand full have been reported. (Jacob et al, 2016, 2017) studied the optical properties and antibacterial properties of lead selenide (PbSe) quantum rods biosynthesized in marine *Aspergillus terreus* and also studied their biomimetic strategies that initiates QD biosynthesis respectively (Jacob et al., 2016, 2017).

Antioxidants are essential for the survival of all living things in fighting and neutralizing free molecular radicals in the body thus reducing, delaying or inhibiting cellular damage (Lobo et al., 2010). Free radicals are associated with oxidative stress, causing damage to the body cells and could lead to numerous diseases, including diabetes, heart disease, cancer etc. (Gebicki, 2016). The formation of free radicals is due to enzymatic and non-enzymatic reactions with oxygen uptake and in addition to that, environmental factors such as pollutants, smoke, sedentary lifestyle and some chemicals also contribute to their formation (Piedrafita et al., 2015; Reuter et al., 2011). Also, organic dyes mostly used in the textile industry produces a lot of toxic effluents that are discharged into the environment. This creates life-threatening problems due to their complex structures that are difficult to biodegrade (Taourati et al., 2020). Photocatalysis by semiconductor nanoparticles are highly investigated environmental nanotechnologies because of their excellent physicochemical properties, biocompatibility and their chemical reaction rate under light irradiation (Weon et al., 2019; Kumaravel and Somasundaram, 2019). These nanomaterials have the ability to destroy unwanted organic compounds in the aqueous phase and eliminate traces of organic species that are stable and difficult to oxidize by conventional water treatments methods (Daghrir et al., 2013).

This research tried to address some of these challenges by evaluating the performance of a novel synthesized PbSe NPs by *Trichoderma* sp. The effects of buffer solution, biomass, pH as well as the ratios of SeO_2 and $Pb(NO_3)_2$ concentrations on PbSe NPs synthesis were studied in detail. The PbSe NPs were characterized by Ultra-visible spectrophotometry (UV–vis) and Transmission electron microscopy (TEM), X-ray diffraction (XRD), Fourier transfer infra-red (FTIR) spectroscopic analysis, Raman spectroscopy and Photoluminescence (PL). The PbSe NPs was further examined for its antioxidant ability with 2,2-diphenyl-1-picrylhydrazyl (DPPH) assay and photocatalytic degradation of Rhodamine B.

2. Materials and methods

2.1. Materials

Selenium dioxide (SeO_2) of 97% and lead nitrate $Pb(NO_3)_2$ of 98.5% purity were purchased from Sinopharm Chemical Regent Beijing Co., Ltd. (China). All other reagents were of analytical grade. The fungus strain, *Trichoderma* sp. WL-Go was cultivated with the modified martin broth medium (MMB medium) containing 1.0 g/L NH_4SO_4, 1.0 g/L KH_2PO_4, 0.5 g/L $MgSO_4{\cdot}7H_2O$ and 5.0 g/L glucose at pH 5.45.

Activation of strain *Trichoderma* sp. WL-Go was performed every two days.

2.2. Biosynthesis of PbSe NPs

Biosynthesis of PbSe NPs begun with growth of *Trichoderma* sp. WL-Go in MMB medium at 30 °C and 150 r/min for 2 days until it reached the late log-phase. Mycelia were then harvested by sieving through a qualitative filter paper (Jiejie Brand-102, 0.15% ash, pore sizes 180 mm, Fushun Dongyang Industry & Trade Limited Company, China) and washed thrice with distilled water and further washed with phosphate buffered saline (PBS) solution. To synthesize PbSe NPs, 0.5 g biomass of strain WL-Go was collected and resuspended in 10 mL PBS at pH 7 containing 1 mM of $Pb(NO_3)_2$ and 1 mM of SeO_2 i.e. (Se:Pb_1:1). The mixture was incubated at 30 °C and 150 rpm for 5 days. After that, the synthesized content was broken by ultrasonication and centrifugated at 3000 rpm for 5 min. The supernatant was collected and separated from the debris. The PbSe NPs in solution were further cleaned thrice with distilled water at 10 000 rpm for 10 min. The obtained NPs were dried at 55 °C for four hours in an oven dryer. Control experiments were performed with the addition of $Pb(NO_3)_2$ and SeO_2 separately. To investigate the effect of pH on PbSe NPs synthesis, synthesis was carried out at different pH, ranging from (5.0–9.0). The pH was obtained by adjusting the proportion of Na_2HPO_4 and NaH_2PO_4 in PBS. Furthermore, different biomass of strain WL-Go wet weight (0.1, 0.3, 0.5 and 1.0) g in 10 mL of PBS were prepared to study the effect of biomass concentration on synthesis of PbSe NPs. Similarly, different concentrations of SeO_2: $Pb(NO_3)_2$ 2 mM in the ratios of (Se: Pb_0.8:1.2, 1:1, 1.2: 0.8) were added to the strain WL-Go and PBS to investigate the effects of SeO_2: $Pb(NO_3)_2$ concentrations on PbSe NPs biosynthesis.

2.3. Characterization of PbSe NPs

PbSe NPs spectrometry was analyzed using a UV–vis spectrophotometer (Metash UV-9000, China). Jasco V-550 UV/VIS spectrophotometer was used to determine absorbance intensities of the powdered Se NPs and PbSe NPs for comparison. Lead (Pb) and selenium (Se) concentrations were determined using inductively coupled plasma optical emission spectrometer (ICP-OES, Perkin-Elmer Optima 2000 DV, USA) and SEM (FEI Quanta 450- USA) was used to access the elemental percentage by Energy-dispersive X-ray spectroscopy (EDS). X-ray diffraction analysis was assessed by diffractometer (XRD, Jasco V-550 UV/VIS spectrophotometer). TEM (FEI Tecnai G220 S-Twin, USA) was used to evaluate morphology of NPs. FTIR spectra of NPs was obtained using a Shimadzu IR Prestige-21 FTIR spectrophotometer (Japan) with the wavelength ranging from 500 to 4000 cm^{-1}. Raman spectroscopy was obtained at room temperature with the Micro spectrometer (Alpha 300 confocal Raman system equipped with a 532 nm laser wavelength. The photoluminescence (PL) spectra was measured with an F-7000 fluorescence spectrometer at the excitation wavelength of 532 nm. All the characterizations were performed with dried PbSe NPs except for UV–vis and ICP analyses.

2.4. Antioxidant ability of Se and PbSe NPs

DPPH assay was performed to measure the antiradical power of the biosynthesized PbSe NPs by reducing the chemical radical DPPH through a hydrogen transfer at room temperature. Varied concentrations of PbSe NPs powder (100–600 g/mL) was prepared in distilled water. A stock solution of 0.1 mM DPPH in methanol was prepared and kept in the dark for an hour prior to the antioxidant test.

For the actual assay, 3 mL of 0.1 mM DPPH methanol plus 1 mL of PbSe NPs was mixed and incubated in the dark for 30 min at room temperature. It was then centrifugated at 8000 rpm for 5 min. The absorbance was then measured at OD 517 nm. DPPH methanol without NPs served as control. And 3 mL of methanol plus 1 mL of distilled water served as the standard. The percentage of inhibition was calculated from the absorbance of sample and control using (Eq. (1)).

$$\text{Scavenging ability (Inhibition \%)} = \frac{Abs(c) - Abs(s)}{Abs(c)} \times 100\% \quad (1)$$

where:

Abs(c) represents Control Absorbance and Abs(s) represents Sample Absorbance

2.5. Photocatalytic test of PbSe NPs

The photocatalytic activity of the PbSe NPs was assessed for its degrading ability against rhodamine B dye- $C_{28}H_{31}ClN_2O_3$ in water at room temperature. Foremost, 50 mg of prepared PbSe NPs was added to rhodamine B (10 mg/L, 50 mL) and then sonicated for 2 min to attain equilibrium. It was then aerated and stirred constantly for 30 min in the presence of 50 W visible halogen light set on near the solution. At 10 min interval, 2 mL of the suspension was collected. All the collected samples were centrifuged at 8000 rpm for 2 min and analyzed with UV–Vis spectrophotometer at a wavelength of 554 nm. The test was conducted at different pH (5, 7 and 9)

The degradation of rhodamine B was calculated by (Eq. (2)) and the kinetic linear fitting curve followed the Langmuir-Hinshelwood apparent first-order kinetics model and calculated by (Eq. (3))

$$\text{Degradation removal rate } (\%) = \frac{(C_o - C)}{C_o} \times 100 \quad (2)$$

$$\text{In}\left(\frac{C_o}{C}\right) = kt \quad (3)$$

where, C_o is the initial concentration of rhodamine B measured after adsorption–desorption equilibrium, C is the concentration at the time (t), and k is the reaction rate kinetic constant.

3. Results and discussion

3.1. Biosynthesis of PbSe NPs

This study presented *Trichoderma* sp. WL-Go in the biosynthesis of PbSe NPs using a benign and cost-effective approach.

Fig. 1(a) shows a schematic diagram to support the speculation on the formation of PbSe NPs. The $Pb(NO_3)_2$ and SeO_2 precursors were transferred into fungal cells during synthesis. SeO_2 was firstly used up by the cells and converted to elemental selenium (Se^0) by the secreted proteins biomolecules. The proteins further acted as reducing biomolecules and converted Se^0 to Se^{2-} which in turn reacted with Pb^{2+} under the catalysis of relative reductase to form PbSe NPs. These proteins further formed a corona around the NPs serving as a capping agent. The reaction produced both intracellular and extracellular PbSe NPs and were considered as a whole for characterization.

The biosynthesis of PbSe NPs in solution was firstly confirmed using UV–vis spectroscopic analyses. In a previous study, extracellular synthesis of selenium nanoparticles (Se NPs) by *Trichoderma* sp. WL-Go culture was optimally achieved at pH 8 (Diko et al., 2019). In the current study, the optimal synthesis of Se NPs in PBS buffer solution was also realized at pH 8 with a vibrant orange color. The Se NPs was subsequently used as the standard for comparison in the synthesis of PbSe NPs as shown in Fig. 1(b). The synthesized PbSe NPs showed a dark grey solution, shown in Fig. 1 (d). The color of the nanoparticles in solution was due to the excitation of the surface plasmon resonance (Ranjitha and Ravishankar, 2018; Schaadt et al., 2005). There was no reaction when only $Pb(NO_3)_2$ was added to strain WL-Go in PBS buffer solution, Fig. 1(c).

3.2. Optimal synthesis conditions of PbSe NPs

UV–vis spectrometry was used to determine the optimal biomass and pH of the synthesized PbSe NPs in solution. The highest absorbance within the visible range was considered as the optimal condition and used for further studies. Foremost, synthesis was carried out at varied biomass 0.1, 0.3, 0.5, 1.0 g/ mL and (Se: Pb_1:1) mM concentration of SeO_2: $Pb(NO_3)_2$ were added simultaneously to the PBS solution at pH 7. As showed in Fig. 2(a), synthesis occurred between 0.3 and 1.0 g biomass of the strain, but 0.5 g recorded the maximum absorbance around 420 nm within the visible range and was used to investigate the optimal pH to carry out PbSe NPs synthesis. Similarly, synthesis was carried out by keeping 0.5 g of biomass and concentration (Se: Pb_1:1) mM constant while varying the pH (5, 6, 7, 8, 9). Analysis of the supernatant indicated that, synthesis occurred in all pH except at pH 5 which had a colorless solution and showed no absorbance in the visible region of the UV–vis spectra. On the other hand, synthesis at pH 9 only synthesized the selenium precursor to form Se NPs and it evidently showed characteristic orange color and absorbance peak at 550 nm (Diko et al., 2019). Synthesis at pH 6, 7 and 8 showed brown to grey solution but pH 8 appeared to have darker solution in comparison to pH 6 and 7. Evidently, pH 8 presented the highest absorbance within the visible range and was used as the optimal pH for further research work. Fig. 2(b) presents the UV–vis spectra and synthesized NPs solutions at different pH values.

The UV–vis spectra of varied concentration ratios have been shown in Fig. 2(c). The absorbance was such that Se: Pb = 0.8:1.2 < 1:1 < 1.2:0.8 which represented 2 mM of the precursor concentrations used. To understand the absorbance within the visible region further, visual analysis was done and it indicated that, an increase in the concentration of the individual precursors by holding the other constant led to visible change i.e. an increase selenium ion concentration led to color change towards brown whilst an increase lead ion concentration led to a dark grey solution as shown in Fig. 3(a). ICP-OES analyses revealed the percental values and confirmed that the color change in synthesized medium was influenced by the quantity of ions in solution, also showed in Fig. 3(b). This also confirmed that, increase in selenium ion concentration led to higher absorbance of the UV–vis spectra by the NPs. EDS further confirmed a similar concentration percental when a (Se: Pb_1:1) mM concentration ratio of the NPs was examined. The detail is shown in Fig. 3(c).

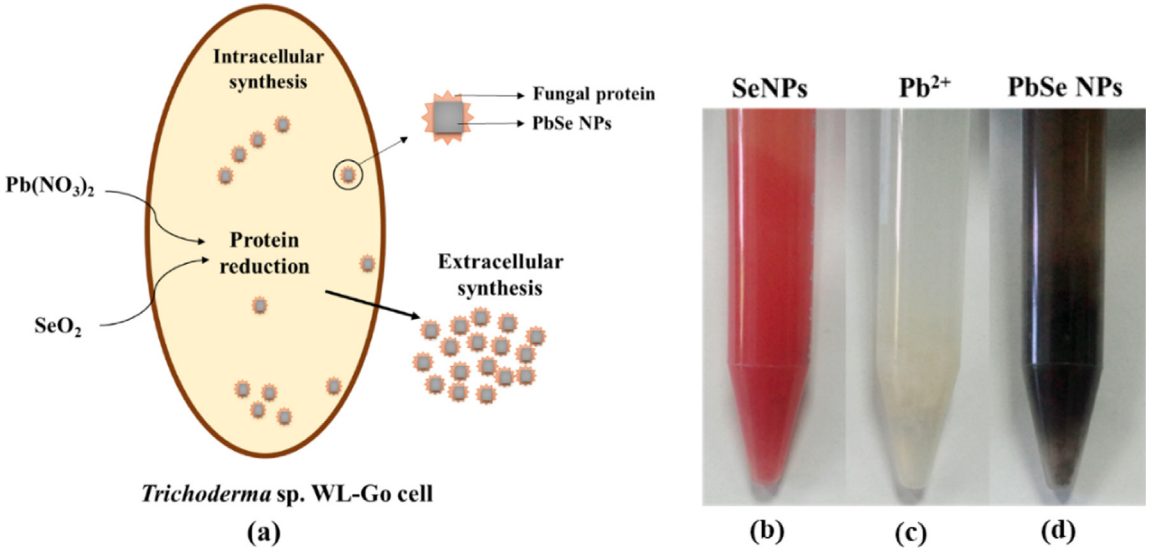

Fig. 1 (a) Schematic fabrication of PbSe NPs by *Trichoderma* sp. WL-Go (b) biosynthesized Se NPs, (c) un-synthesized $Pb(NO_3)_2$ and (d) biosynthesized PbSe NPs in solution.

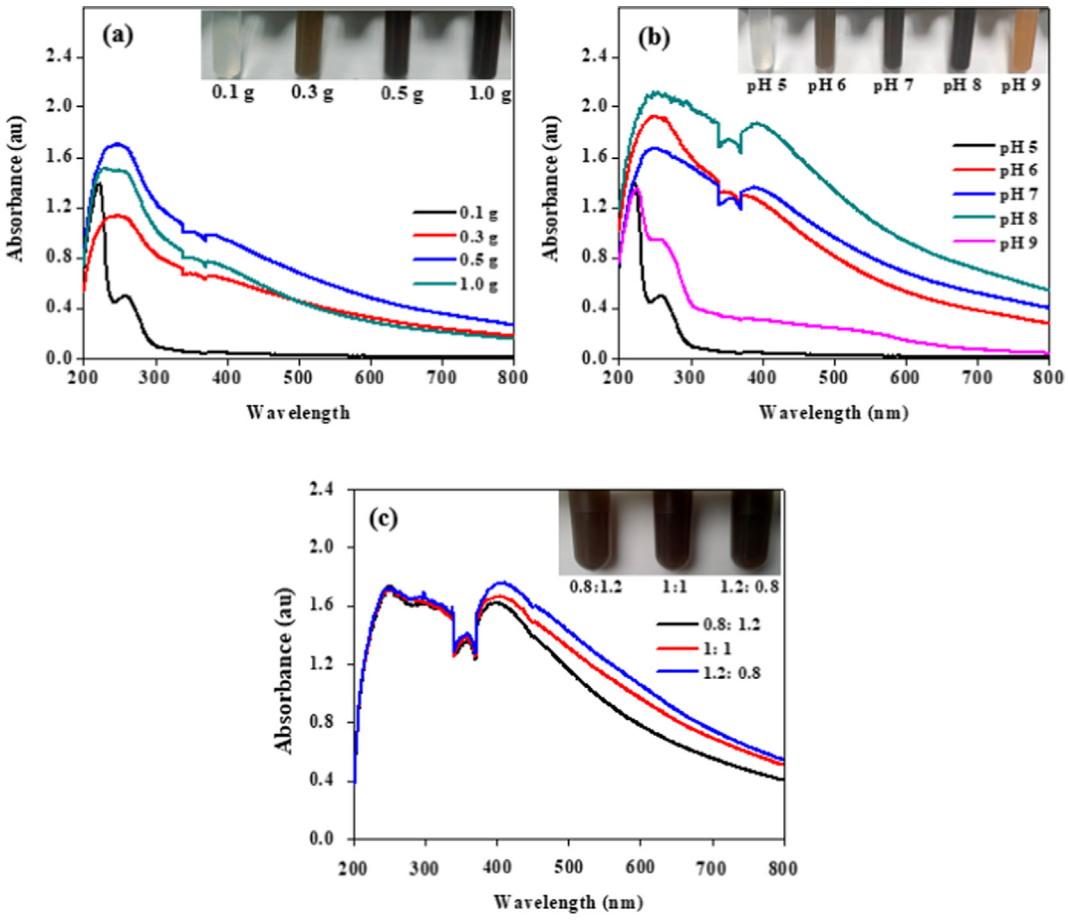

Fig. 2 SPR analysis of biosynthesized PbSe NPs in solution (a) in different biomass, (b) varied pH and (c) different concentration ratios of SeO_2: $Pb(NO_3)_2$_2 mM.

3.2.1. Absorbance of powdered Se NPs and PbSe NPs by UV–vis analysis

Powdered UV–vis analysis proved that the PbSe NPs exhibited better absorbance within the visible region than Se NPs which served as the standard, as shown in Fig. 4(a). This indicates that the PbSe nanocomposite might have better performance in its applications. Fig. 4(b) showed the bandgap of Se NPs and PbSe NPs corresponding to 1.88 eV and 1.5 eV respectively. The bandgap of PbSe NPs was much higher than that of the bulk PbSe (0.27 eV) (Krishna et al., 2018) and also biosynthesized PbSe quantum rods by *Aspergillus terreus* with a bandgap of (1.25 eV) (Mary Jacob et al., 2014). It has been established that the properties of a semiconductor are dependent on the structure and the value of its bandgap which can increase the lifespan of photoinduced electrons and holes (Khataee et al., 2015a). Most importantly, a change in bandgap has been reported to lead to decrease in crystal size of nanocomposite which has a relation with quantum confinement effect, thus enhancing photocatalytic activity (Nahyoon et al., 2019).

3.2.2. Transmission electron microscopy

The synthesized nanoparticles were characterized by TEM to ascertain morphologies and the sizes of the NPs. In Fig. 5 (a), the Se NPs indicated that, the nanoparticles were spherical in shape with sizes ranging from 80 to 180 nm with the highest frequency occurring at 120 nm as shown in Fig. 5(b). The spherical nature of the nanoparticles is common of synthesized Se NPs and have been reported elsewhere (Diko et al., 2019). On the other hand, as indicated in Fig. 5(c), the semiconductor NPs of PbSe resulted in smaller cubic shaped nanoparticles which ranged from 10 to 30 nm capped by proteins biomacromolecules secreted by strain WL-Go. The nanoparticle sizes with the maximum occurrence was around 15 nm as shown in Fig. 5(d). Many researches have suggested PbSe NPs or quantum dots as cubic which is as result of facets formed by both Pb and Se atoms (Khataee et al., 2015a; Chiu et al., 2019; Hosseinpour-Mashkani et al., 2014). This nanocomposite allowed for the creation of a new form of biomaterial whose features and dynamics were influenced by the synergy between Se and Pb ions in the presence of secreted proteins by strain WL-Go.

3.2.3. X-ray diffraction analysis

XRD analysis was further used to confirm the formation of the NPs. As shown in Fig. 6(a), the Se NPs revealed peaks of 100, 101 and 102 at 2θ relating and are attributed to the formation of spherical crystalline nanoparticles (Khiralla and El-Deeb, 2015). The XRD patterns for the different concentration ratio of the PbSe NPs (0.8:1.2, 1:1, 1.2:0.8) as shown in Fig. 6(b), exhibited a wide range of peaks at 2θ i.e. 111, 200, 220, 311,

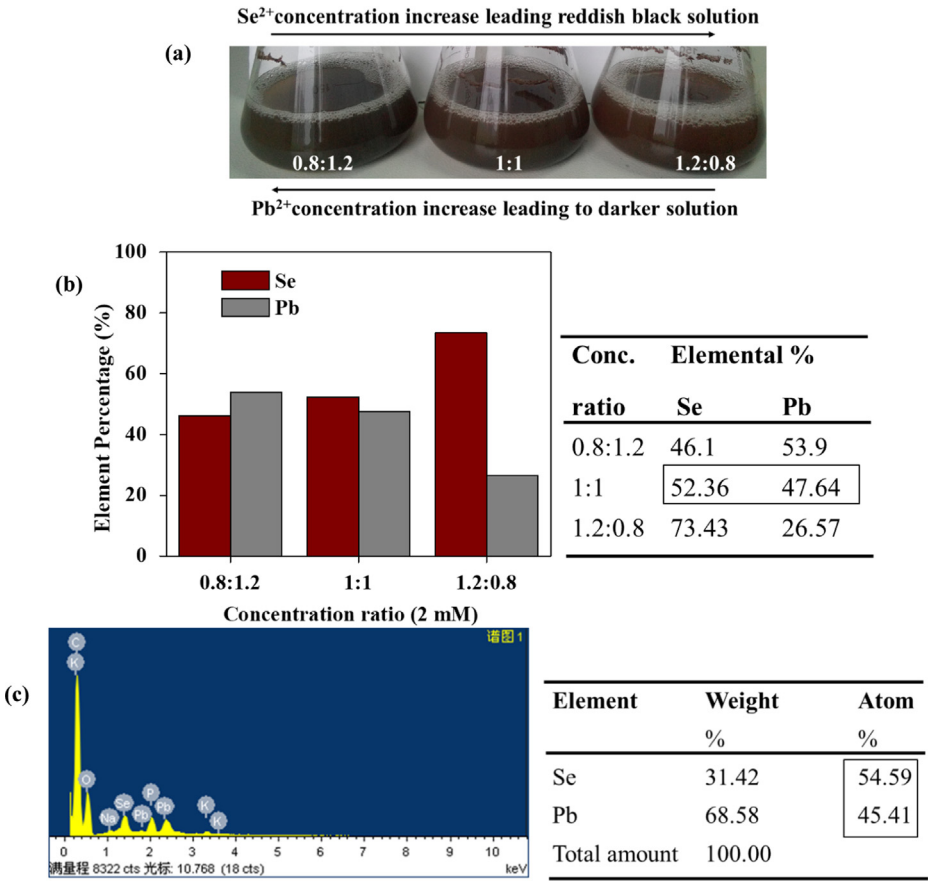

Conc. ratio	Elemental % Se	Pb
0.8:1.2	46.1	53.9
1:1	52.36	47.64
1.2:0.8	73.43	26.57

Element	Weight %	Atom %
Se	31.42	54.59
Pb	68.58	45.41
Total amount	100.00	

Fig. 3 (a) Visual color observation with respect to increase concentrations SeO_2 or $Pb(NO_3)_2$ of PbSe NPs in solution (b) ICP-OES elemental percentage analysis, (c) EDS elemental percentage of PbSe NPs_ Se: Pb = 1:1 varied concentration.

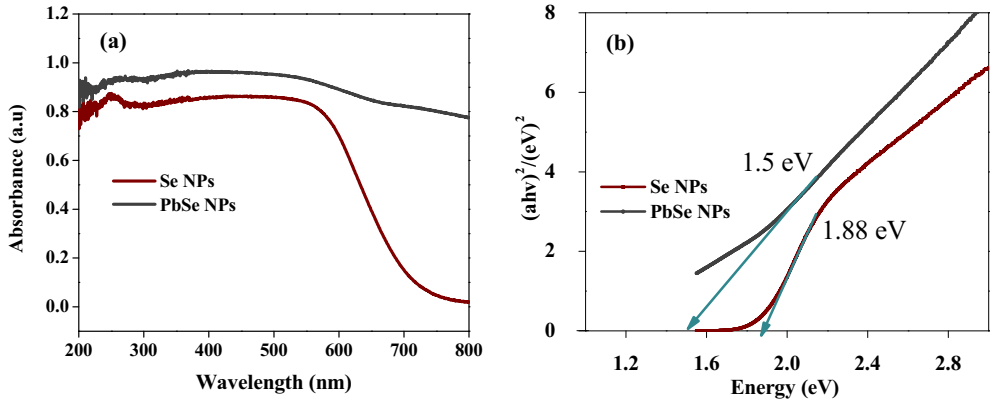

Fig. 4 (a) Powdered UV–vis analysis and (b) Bandgap of Se NPs and PbSe NPs.

222, 400, 331 and 420 reflections which corresponds to the clausthalite crystal phase of lead selenide (PbSe) (Zhu et al., 2015). Moreover, these strong peaks showed good crystallization of the synthesized samples and have been attributed to the formation of face center cubic (fcc) structured nanoparticles (Chen et al., 2016; Fan et al., 2015; Bhat et al., 2019). These observations further confirm that PbSe NPs were successfully synthesized by *Trichoderma* sp. WL-Go

3.2.4. Fourier transfer infra-red spectroscopy

FTIR spectroscopy was used to examine the surface chemistry and identify functional groups responsible for synthesis and capping of NPs. As shown in Fig. 7(a), both Se NPs and PbSe NPs displayed peaks of alkenes (C═C) at 1638 cm^{-1} and 1659 cm^{-1}, alkane (C—H) at 2949 cm^{-1} and alcohol (O—H) peaks at 3325 cm^{-1}. These medium to strong peaks have been observed in the synthesis of other nanoparticles and were vital

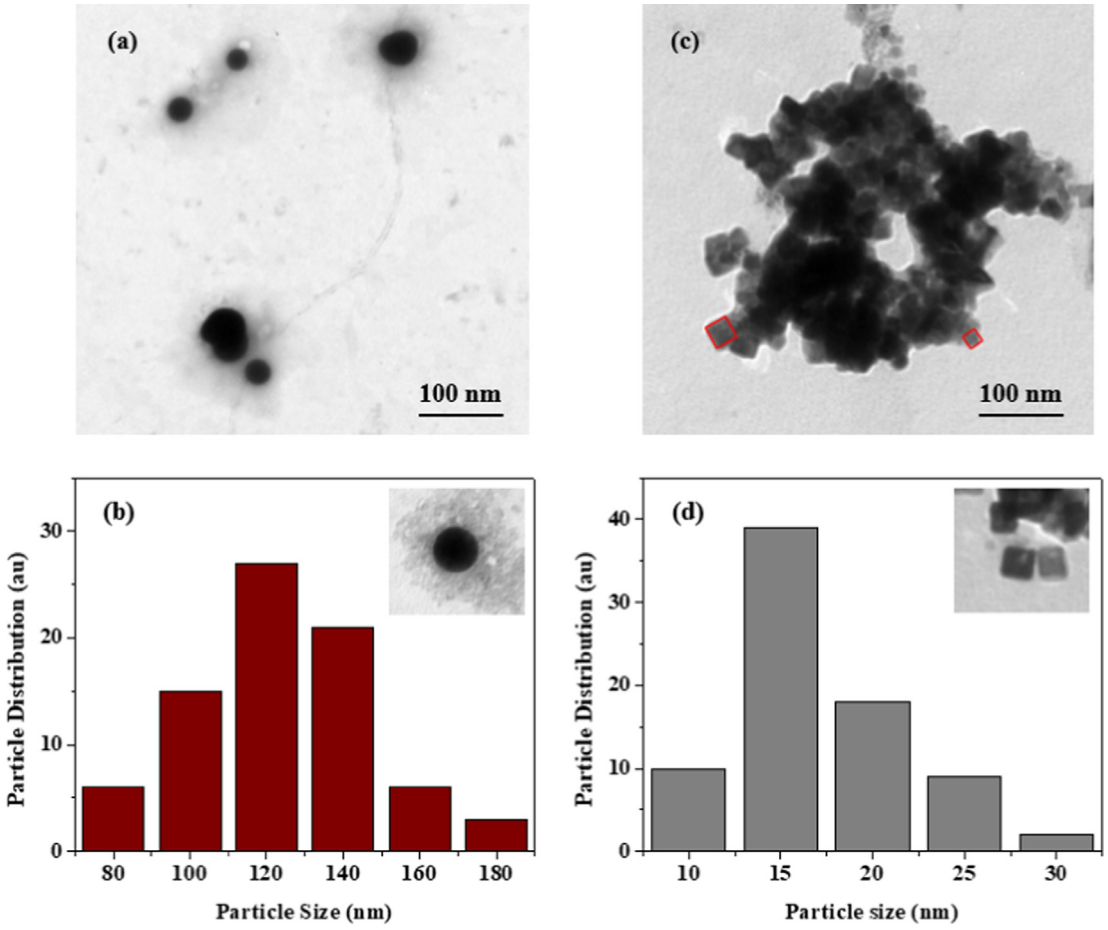

Fig. 5 Se NPs (a) Morphological and (b) size distribution analysis and PbSe NPs (c) morphological and (d) size distribution analysis.

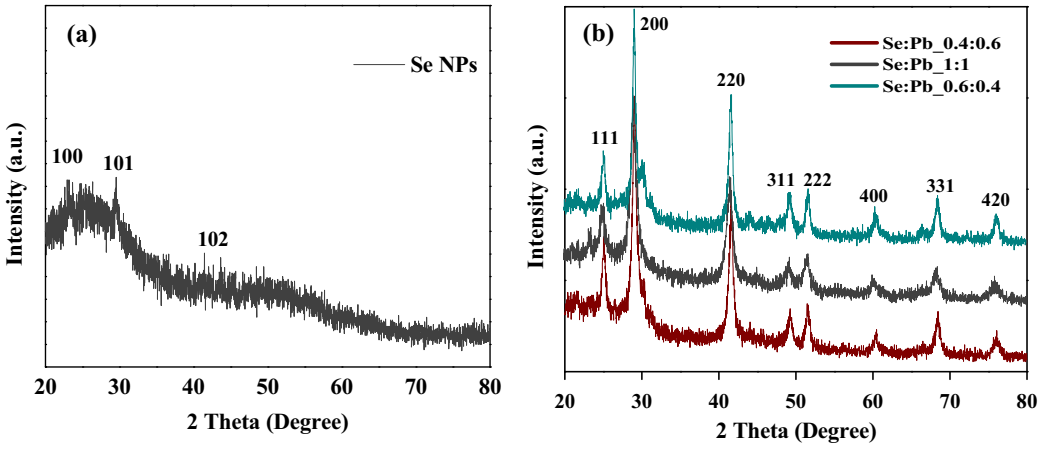

Fig. 6 XRD analysis of (a) Se NPs and (b) varied concentration ratio of PbSe NPs.

in the formation and capping of the NPs (Rajendran and Sen, 2018; Rahman et al., 2014; Tugarova et al., 2018). Proteins secreted by fungus during synthesis of nanomaterials are biodegradable and can produce reducing sugars and bio-conjugates that combine the bioactive compounds to the surface of the nanomaterials yielding stabilized nanoproducts (Jacob et al., 2017; Castro-Longoria et al., 2011; Ranoszek-Soliwoda et al., 2019), with unique application properties. These results suggest the prominent involvement of proteins in biosorption and bio-reduction of the Pb and Se precursors by the fungus (Jacob et al., 2017).

3.2.5. Raman spectroscopy

Raman spectroscopy has vibrational detecting and phonon modes abilities to identify single molecules in samples to

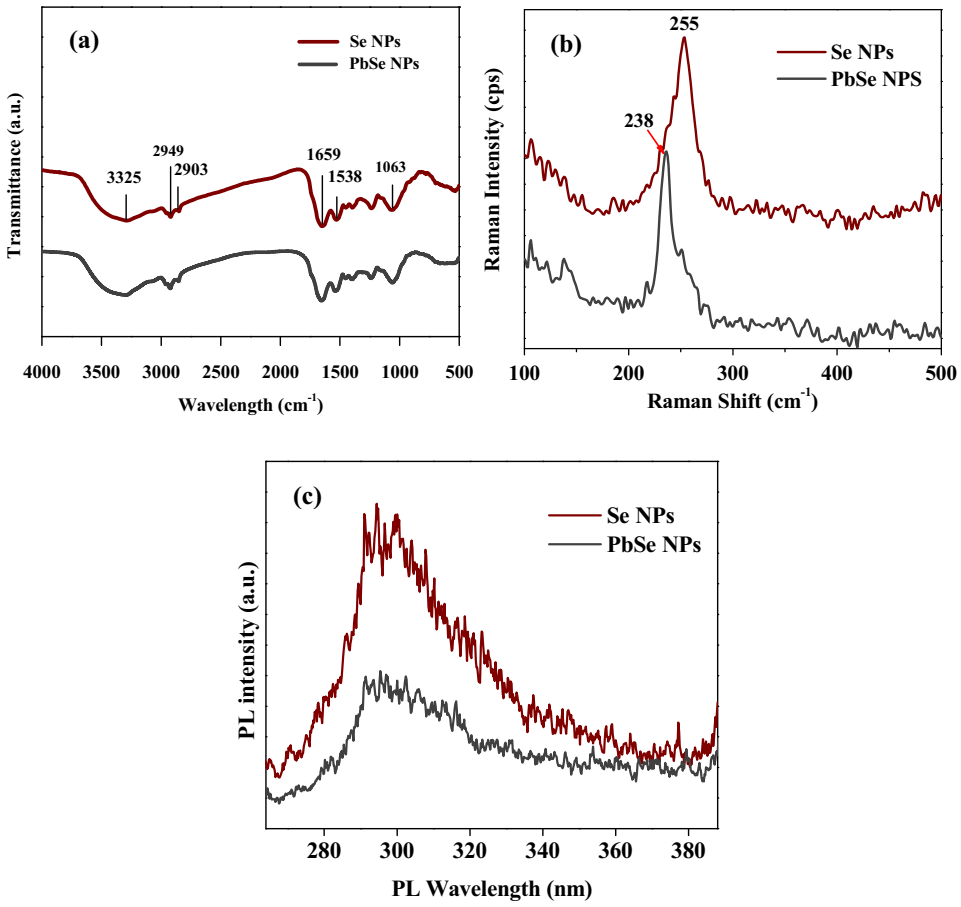

Fig. 7 (a) FTIR spectra, (b) Raman and (c) Photoluminescence analysis of Se NPs and PbSe NPs.

ascertain the chemical compositions of crystalline structures by assigning new vibrational bands/shifts to the examined nanomaterials and other extraneous phases or areas with a local order/disorder of the crystalline lattice (Flores-Valenzuela et al., 2015; Gupta et al., 2020). The synthesized PbSe NPs was subjected to Raman spectroscopy to further assess the vibration of the nanostructured material.

As illustrated in Fig. 7(b), Se NPs showed wavelength of ~255 cm^{-1} and PbSe NPs showed wavelengths of ~238 cm^{-1}. The presence of the Raman peak at 255 cm^{-1} has been attributed to the bond-stretching vibration of the disordered Se chains and rings in the range of the mean coordination number (Iaseniuc et al., 2018). Similarly, ZnSe nanostructures showed a peak positioned at around 253 cm^{-1} which was attributed to the transverse optic (TO) and longitudinal optic (LO) phonon modes of ZnSe nanoparticles and it was indicated that an uncompleted reaction of confined semiconductors could have occurred leading to strong resonance of the LO mode as a result of Frölich interaction (Li et al., 2010). Another LO band was assigned to 252 cm^{-1} band (Arivazhagan et al., 2014). The band at 238 cm^{-1} reportedly is a weak band with a consistent trend of progressive breaking of Se-chains (Iovu et al., 2005). The presence of selenium (Se) atoms might have played a role in the blueshift of Raman band from 255 cm^{-1} of the Se NPs to 238 cm^{-1} of the PbSe NPs at a lower intensity.

3.2.6. Photoluminescence (PL) Spectroscopy

There is a direct link between PL intensity and recombination rate of photogenerated electron-hole pairs which leads to low PL intensity with lower recombination rate, thereby enhancing photocatalytic performance (Nahyoon et al., 2019). Shown in Fig. 7(c), the PL emission spectra of the Se NPs exhibited was slightly asymmetric at excitation wavelength of 294 nm. The PbSe NPs, also asymmetric, showed a single emission peak at 296 nm with reduced intensity in comparison to Se NPs. This emission pattern has been linked to the change in the concentration of charge carriers and recombination of photoexcited electrons and holes (Nahyoon et al., 2019; Li et al., 2018). PbSe NPs with reduced PL intensity might be due to the suppression of exciton PL by the presence of extra holes introduced by the Pb^{2+}.

3.3. Antioxidant activity of PbSe NPs

DPPH assay based on electron-transfer produces a violet solution in methanol/ethanol. This free radical, stabilized at room temperature, can be reduced in the presence of an antioxidant molecules given rise to a yellow solution. Selenium has been known to possess antioxidant ability (Vyas and Rana, 2017a, 2017b) and could counter the effects of free radicals (Munné-Bosch and Pintó-Marijuan, 2017). PbSe NPs was investigated to assess its performance against free radicals, with Se NPs as

the standard for comparison. The increase in the concentration of the NPs was proportional to the inhibition rate in the DPPH methanol solution as shown in Fig. 8. Fig. 8(b) showed a better reduction performance of PbSe NPs over Se NPs in Fig. 8(a) with the addition of the same concentration of NPs. As shown in Fig. 8(c), the Se NPs showed an inhibition percentage of 65.98% upon the addition of 600 g/mL. On the other hand, 86.37% inhibition was realized with the addition of 200 g/mL of PbSe NPs and then slightly increased to 88.60% at 600 g/mL addition. Biogenic SnO_2 NPs reported an inhibition percentage of about 55% on DPPH with the addition of 200 g/mL (Vidhu and Philip, 2015). All in all, the addition of selenium enhanced the performance of the PbSe semiconductor NPs, providing an easy and rapid way to evaluate the antioxidants performance by PbSe NPs.

3.4. Photocatalytic activity analyses of PbSe NPs

Photocatalytic activity depends on phase structure, optical absorbance and adsorption capacity of photocatalyst. This heterostructure influences the separation of electrons/holes pairs in photocatalysts(Zhu et al., 2015). PbSe NPs demonstrated good photodegradation activity against rhodamine B under visible light at ambient temperature. The photocatalytic degradation of rhodamine B under visible light obeyed pseudo-first-order kinetics with respect to the concentration of rhodamine B. UV–vis spectrometry recorded at 554 nm showed the decomposition activity from 0 to 30 min. A gradual decline in absorbance peak was observed in the presence of PbSe NPs with increased exposure time. This led to a decrease in the concentrations of rhodamine B dye with significant degradation of 54%, 48% and 82% corresponding to pH 5 pH 7 and pH 9 respectively, shown in Fig. 9(a). It is seen that, pH 9 further enhanced the photocatalytic performance of the PbSe NPs after 30 min. It has been shown that nanoparticles aggregate at certain pH values and decreases the available active surface sites with little degradation at neutral pH but with enhanced degradation percentage in the acid or basic solution (Alfredo Reyes Villegas et al., 2020). The degradation ability has been attributed to oxidation by the reactive oxygen species (ROS) with the capability to oxidize the organic dye to yield H_2O and CO_2 molecules (Nahyoon et al., 2019; Zhu et al., 2015). Also, the hydroxyl groups absorbed on the surface of the catalyst by attacking organic compounds (Khataee et al., 2015a). Fig. 9(b) shows the linear relationship/ pseudo-first-order kinetic at different pH of the degradation of rhodamine B by PbSe NPs with good correlation. The kinetic parameters are also shown in Table 1.

The mechanism of PbSe semiconductor NPs for rhodamine B photodegradation has been shown in a proposed schematic diagram in Fig. 9(c). Here, a light source is placed near the PbSe NPs surface and electron excitation occurs. The charged electrons in the valance band (VB) travels to the conduction band (CB) thereby leaving charged holes in valance band. The holes in valence band of the NPs reacts with water molecules (H_2O)/ hydroxyl ions (OH) and yields hydroxyl radicals (OH·) (Reddy et al., 2017). Acting as an oxidizing agent, the hydroxyl radicals (OH·) breaks down the rhodamine B dye

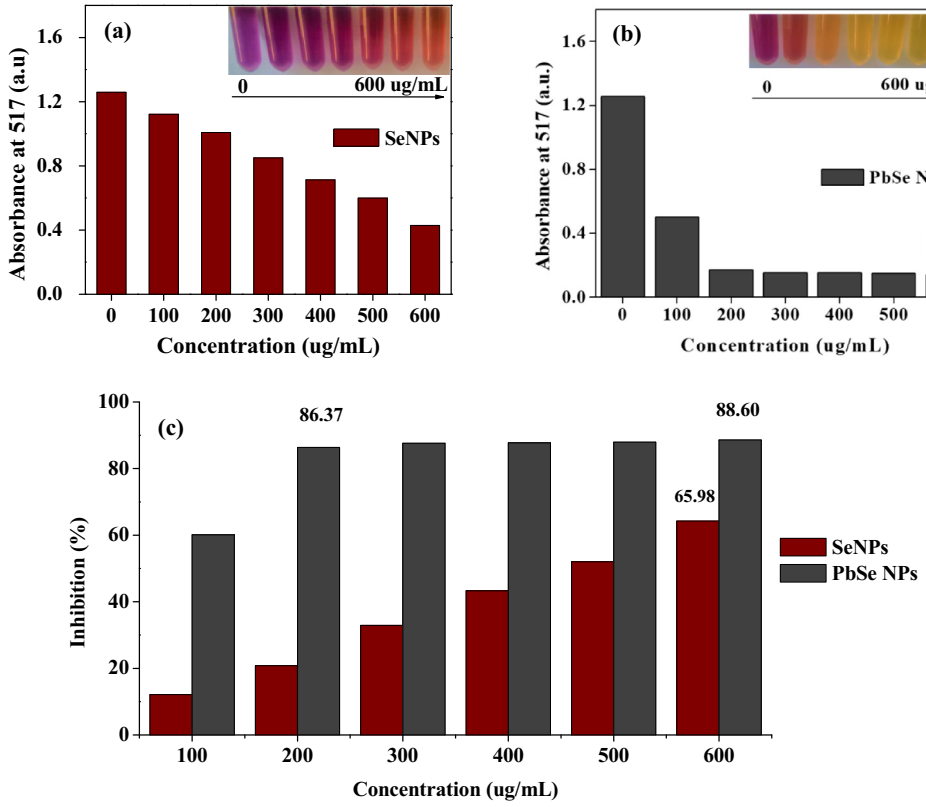

Fig. 8 Antioxidant activity of synthesized (a) Se NPs at OD 517, (b) PbSe NPs at OD 517 and (c) inhibition percentage comparison of Se NPs and PbSe NPs.

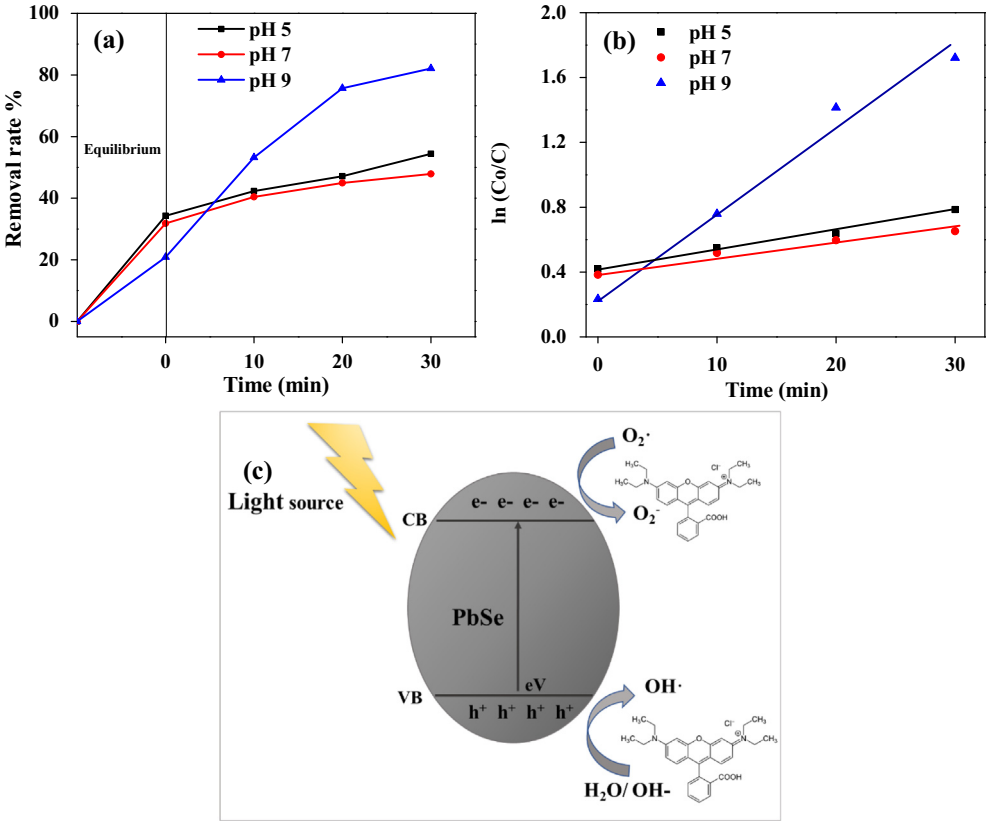

Fig. 9 Photocatalytic activity of PbSe NPs for the degradation of rhodamine B under (a) visible light irradiation and (b) pseudo-first-order kinetic plots of rhodamine B, (c) schematic photocatalytic mechanism of PbSe NPs in degrading rhodamine B.

Table 1 Pseudo-first-order kinetic parameters for the degradation of rhodamine B (10 mg/L) with Lead selenide nanoparticles (PbSe NPs) under different pH conditions.

pH	K (min^{-1})	R^2
5	0.0118	0.9912
7	0.0089	0.9604
9	0.0512	0.9824

and produces superoxide with a good affinity towards the PbSe semiconductor NPs. Similarly, the introduction of peroxydisulfate ion to the photocatalytic system hindered the recombination of photo-generated electrons and holes which led to heightened degradation of organic pollutants (Khataee et al., 2015a).

4. Conclusion

Lead selenide nanoparticles were synthesized for the first time by the *Trichoderma* sp. WL-Go at pH 8, 0.5 g biomass of strain WL-Go and (1:1) mM_SeO_2: $Pb(NO_3)_2$ concentration as the optimal synthesis condition. The characterization of PbSe NPs by UV–vis, TEM, XRD, FTIR, Raman and PL showed (10–30) nm cubic face centered particles capped by proteins secreted by strain WL-Go. Further, PbSe NPs showed Raman band at 238 cm^{-1} and low electron-hole pairs recombination PL intensity of 296 nm. The PbSe NPs demonstrated significant antioxidant activity of 88.60% and photocatalytic activity of 82% in 30 min in degrading rhodamine B dye (10 mg/L, 50 mL). The creation of the bio PbSe semiconductor NPs was simple and benign and could be exploited for its antioxidant potential and water remediation capabilities.

Acknowledgments

This work was supported by the Open Project of State Key Laboratory of Urban Water Resource and Environment, Harbin Institute of Technology (No. QAK201943), the National Natural Science Foundation of China (No. 31970107) and DUT International Students Presidential Scholarship.

Compliance with Ethical Standards

Conflict of interest: The authors declare that they have no conflict of interest.

Ethical approval: This article does not contain any studies with human participants or animals performed by any of the authors.

References

Alfredo Reyes Villegas, V., Isaías De León Ramírez, J., Hernandez Guevara, E., Perez Sicairos, S., Angelica Hurtado Ayala, L., Landeros Sanchez, B., 2020. Synthesis and characterization of magnetite nanoparticles for photocatalysis of nitrobenzene. J.

Saudi Chem. Soc. 24, 223–235. https://doi.org/10.1016/j.jscs.2019.12.004.

Ali, A., Zafar, H., Zia, M., Haq, I. ul, Phull, A.R., Ali, J.S., Hussain, A., 2016. Synthesis, characterization, applications, and challenges of iron oxide nanoparticles. Nanotechnol. Sci. Appl. 9, 49–67 https://doi.org/10.2147/NSA.S99986.

Alruqi, S.S., AL-Thabaiti, S.A., Khan, Z., 2019. Iron-nickel bimetallic nanoparticles: surfactant assisted synthesis and their catalytic activities. J. Mol. Liq. 282, 448–455 https://doi.org/10.1016/j.molliq.2019.03.021.

Anwar, Sharmistha, Anwar, Shahid, Mishra, B.K., 2015. Effect of bath temperature on PbSe thin films prepared by chemical synthesis. Mater. Sci. Semicond. Process. 40, 910–916 https://doi.org/10.1016/j.mssp.2015.07.077.

Arivazhagan, V., Parvathi, M.M., Rajesh, S., 2014. Complementary NIR absorption of ZnSe induced by multiple PbSe submonolayers by vacuum deposition technique. Vacuum 99, 95–98 https://doi.org/10.1016/j.vacuum.2013.05.001.

Bhat, T.S., Kalekar, A.S., Dalavi, D.S., Revadekar, C.C., Khot, A.C., Dongale, T.D., Patil, P.S., 2019. Hydrothermal synthesis of nanoporous lead selenide thin films: photoelectrochemical and resistive switching memory applications. J. Mater. Sci.: Mater. Electron. 30, 17725–17734 https://doi.org/10.1007/s10854-019-02122-1.

Castro-Longoria, E., Vilchis-Nestor, A.R., Avalos-Borja, M., 2011. Biosynthesis of silver, gold and bimetallic nanoparticles using the filamentous fungus *Neurospora crassa*. Colloids Surfaces B Biointerfaces 83, 42–48. https://doi.org/10.1016/j.colsurfb.2010.10.035.

Chen, X., Zhu, Y.-B., Xing, Z., Tang, G., Fan, H., 2016. Synthesis of PbSe nanostructures with different size and morphology and their electrochemical properties. J. Mater. Sci.: Mater. Electron. 27, 1151–1157 https://doi.org/10.1007/s10854-015-3864-8.

Chiu, M.S., Lin, C.C., Lee, A.T., Huang, Y.C., Huang, M.H., 2019. Aqueous-phase synthesis of size-tunable PbSe nanocubes at room temperature for optical property characterization. Chem. – A Eur. J. 25, 367–372. https://doi.org/10.1002/chem.201804631.

Daghrir, R., Drogui, P., Robert, D., 2013. Modified TiO_2 for environmental photocatalytic applications: a review. Ind. Eng. Chem. Res. 52, 3581–3599. https://doi.org/10.1021/ie303468t.

Diko, C.S., Zhang, H., Lian, S., Fan, S., Li, Z., Qu, Y., 2019. Optimal synthesis conditions and characterization of selenium nanoparticles in *Trichoderma* sp. WL-Go culture broth. Mater. Chem. Phys. 122583.

Fan, H., Su, T., Li, H., Du, B., Liu, B., Sun, H., Zhang, Y., Li, L., Li, S., Hu, M., Ma, H., Jia, X., 2015. Enhanced thermoelectric performance of PbSe co-doped with Ag and Sb. J. Alloys Compd. 639, 106–110 https://doi.org/10.1016/j.jallcom.2015.03.117.

Flores-Valenzuela, J., Cortez-Valadez, M., Ramírez-Bon, R., Arizpe-Chavez, H., Román-Zamorano, J.F., Flores-Acosta, M., 2015. Optical and vibrational properties of PbSe nanoparticles synthesized in clinoptilolite. Phys. E Low-dimensional Syst. Nanostruct. 72, 1–6 https://doi.org/10.1016/j.physe.2015.04.012.

Gebicki, J.M., 2016. Oxidative stress, free radicals and protein peroxides. Arch. Biochem. Biophys. 595, 33–39 https://doi.org/10.1016/j.abb.2015.10.021.

Gervas, C., Mlowe, S., Revaprasadu, N., 2016. Synthesis of PbTe and PbSe nanoparticles under the influence of hydrochloric acid and carbon dioxide. Mater. Sci. Semicond. Process. 56, 295–301 https://doi.org/10.1016/j.mssp.2016.09.001.

Guilger-Casagrande, M., Germano-Costa, T., Pasquoto-Stigliani, T., Fraceto, L.F., de Lima, R., 2019. Biosynthesis of silver nanoparticles employing *Trichoderma harzianum* with enzymatic stimulation for the control of Sclerotinia sclerotiorum. Sci. Rep. 9, 1–9. https://doi.org/10.1038/s41598-019-50871-0.

Gupta, R., Chauhan, R.P., Kumar, R., 2020. Influence of gamma radiation on the optical, morphological, structural and electrical properties of electrodeposited lead selenide nanowires. Opt. Mater. (Amst). 99, 109538.

Han, X., Han, W., Zhang, S., Liu, Z., Fu, G., 2019. PEGylation of protein-imprinted nanocomposites sandwiching CdTe quantum dots with enhanced fluorescence sensing selectivity. RSC Adv. 9, 38165–38173. https://doi.org/10.1039/c9ra08556d.

Horta, M.A.C., Filho, J.A.F., Murad, N.F., De Oliveira Santos, E., Dos Santos, C.A., Mendes, J.S., Brandão, M.M., Azzoni, S.F., De Souza, A.P., 2018. Network of proteins, enzymes and genes linked to biomass degradation shared by *Trichoderma* species. Sci. Rep. 8, 1–11. https://doi.org/10.1038/s41598-018-19671-w.

Hosseinpour-Mashkani, S.M., Ramezani, M., Vatanparast, M., 2014. Synthesis and characterization of lead selenide nanostructure through simple sonochemical method in the presence of novel precursor. Mater. Sci. Semicond. Process. 26, 112–118. https://doi.org/10.1016/j.mssp.2014.04.016.

Iaseniuc, O.V., Iovu, M.S., Ghiulnare, A., Mesterca, R., Jderu, A., Enachescu, M., 2018. Micro-Raman spectra of bulk GexAsxSe1-2X chalcogenide glasses. Proc. Rom. Acad. Ser. A – Math. Phys. Tech. Sci. Inf. Sci. 19, 545–550. https://doi.org/10.1117/12.2323655.

Iovu, M.S., Kamitsos, E.I., Varsamis, C.P.E., Boolchand, P., Popescu, M., Hellenic, N., 2005. Raman spectra of AsxSe100-x and $As_{40}Se_{60}$ glasses doped with metals. Chalcogenide Lett. 2, 21–25.

Jacob, J.M., Raj Mohan, B., Akshay Gowda, K.M., 2016. Insights into the optical and anti-bacterial properties of biogenic PbSe quantum rods. J. Saudi Chem. Soc. 20, 480–485 https://doi.org/10.1016/j.jscs.2014.10.008.

Jacob, J.M., Sharma, S., Balakrishnan, R.M., 2017. Exploring the fungal protein cadre in the biosynthesis of PbSe quantum dots. J. Hazard. Mater. 324, 54–61 https://doi.org/10.1016/j.jhazmat.2015.12.056.

Khataee, A., Arefi-Oskoui, S., Fathinia, M., Esmaeili, A., Hanifehpour, Y., Joo, S.W., Hamnabard, N., 2015a. Synthesis, characterization and photocatalytic properties of Er-doped PbSe nanoparticles as a visible light-activated photocatalyst. J. Mol. Catal. A: Chem. 398, 255–267 https://doi.org/10.1016/j.molcata.2014.11.009.

Khataee, A., Arefi-Oskoui, S., Fathinia, M., Fazli, A., Shahedi Hojaghan, A., Hanifehpour, Y., Joo, S.W., 2015b. Photocatalysis of sulfasalazine using Gd-doped PbSe nanoparticles under visible light irradiation: kinetics, intermediate identification and phytotoxicological studies. J. Ind. Eng. Chem. 30, 134–146 https://doi.org/10.1016/j.jiec.2015.05.014.

Khiralla, G.M., El-Deeb, B.A., 2015. Antimicrobial and antibiofilm effects of selenium nanoparticles on some foodborne pathogens. LWT – Food Sci. Technol. 63, 1001–1007. https://doi.org/10.1016/j.lwt.2015.03.086.

Kolahalam, L.A., Kasi Viswanath, I.V., Diwakar, B.S., Govindh, B., Reddy, V., Murthy, Y.L.N., 2019. Review on nanomaterials: synthesis and applications. Mater. Today: Proc. 18, 2182–2190 https://doi.org/10.1016/j.matpr.2019.07.371.

Krishna, V.D., Wu, K., Su, D., Cheeran, M.C.J., Wang, J.-P., Perez, A., 2018. Nanotechnology: review of concepts and potential application of sensing platforms in food safety. Food Microbiol. 75, 47–54 https://doi.org/10.1016/j.fm.2018.01.025.

Kumar, S., Nehra, M., Deep, A., Kedia, D., Dilbaghi, N., Kim, K.-H., 2017. Quantum-sized nanomaterials for solar cell applications. Renew. Sustain. Energy Rev. 73, 821–839 https://doi.org/10.1016/j.rser.2017.01.172.

Kumaravel, V., Somasundaram, S., 2019. Exploitation of Nanoparticles as Photocatalysts for Clean and Environmental Applications. .

Li, H., Wang, B., Li, L., 2010. Study on Raman spectra of zinc selenide nanopowders synthesized by hydrothermal method. J. Alloys Compd. 506, 327–330 https://doi.org/10.1016/j.jallcom.2010.06.201.

Li, M., Luo, J., Fu, C., Kan, H., Huang, Z., Huang, W., Yang, S., Zhang, J., Tang, J., Fu, Y., Li, H., Liu, H., 2018. PbSe quantum dots-based chemiresistors for room-temperature NO_2 detection.

Sens. Actuators B Chem. 256, 1045–1056 https://doi.org/10.1016/j.snb.2017.10.047.

Lobo, V., Patil, A., Phatak, A., Chandra, N., 2010. Free radicals, antioxidants and functional foods: Impact on human health. Pharmacogn. Rev. 4, 118–126. https://doi.org/10.4103/0973-7847.70902.

Malarkodi, C., Rajeshkumar, S., Paulkumar, K., Jobitha, G.G., Vanaja, M., Annadurai, G., 2013. Biosynthesis of semiconductor nanoparticles by using sulfur reducing bacteria *Serratia nematodiphila*. Adv. Nano Res. 1, 83–91 https://doi.org/10.12989/anr.2013.1.2.083.

Malarkodi, C., Rajeshkumar, S., Paulkumar, K., Vanaja, M., Gnanajobitha, G., Annadurai, G., 2014. Biosynthesis and antimicrobial activity of semiconductor nanoparticles against oral pathogens. Bioinorg. Chem. Appl. 2014. https://doi.org/10.1155/2014/347167.

Mary Jacob, J., Balakrishnan, R.M., Kumar, U.B., 2014. Biosynthesis of lead selenide quantum rods in marine *Aspergillus terreus*. Mater. Lett. 124, 279–281. https://doi.org/10.1016/j.matlet.2014.03.106.

Munné-Bosch, S., Pintó-Marijuan, M., 2017. Free radicals, oxidative stress and antioxidants. In: Thomas, B., Murray, B.G., Murphy, D. J.B.T.-E. of A.P.S. (Second E. (Eds.), Academic Press, Oxford, pp. 16–19. https://doi.org/10.1016/B978-0-12-394807-6.00077-0.

Nahyoon, N.A., Liu, L., Rabé, K., Nahyoon, S.A., Abro, A.H., Yang, F., 2019. Efficient degradation of rhodamine B with sustainable electricity generation in a photocatalytic fuel cell using visible light Ag_3PO_4/Fe/GTiP photoanode and $ZnIn_2S_4$ photocathode. J. Taiwan Inst. Chem. Eng. 96, 137–147 https://doi.org/10.1016/j.jtice.2018.10.019.

Panda, S.S., Katz, H.E., Tovar, J.D., 2018. Solid-state electrical applications of protein and peptide based nanomaterials. Chem. Soc. Rev. 47, 3640–3658. https://doi.org/10.1039/C7CS00817A.

Paszkiewicz, M., Gołąbiewska, A., Rajski, Ł., Kowal, E., Sajdak, A., Zaleska-Medynska, A., 2016. Synthesis and characterization of monometallic (Ag, Cu) and bimetallic Ag-Cu particles for antibacterial and antifungal applications. J. Nanomater. 2016. https://doi.org/10.1155/2016/2187940.

Piedrafita, G., Keller, M.A., Ralser, M., 2015. The impact of non-enzymatic reactions and enzyme promiscuity on cellular metabolism during (Oxidative) stress conditions. Biomolecules 5, 2101–2122. https://doi.org/10.3390/biom5032101.

Qu, X., Alvarez, P.J.J., Li, Q., 2013. Applications of nanotechnology in water and wastewater treatment. Water Res. 47, 3931–3946 https://doi.org/10.1016/j.watres.2012.09.058.

Qu, Y., Li, X., Lian, S., Dai, C., Jv, Z., Zhao, B., Zhou, H., 2018. Biosynthesis of gold nanoparticles using fungus *Trichoderma* sp. WL-Go and their catalysis in degradation of aromatic pollutants. IET Nanobiotechnol. 13, 12–17. https://doi.org/10.1049/iet-nbt.2018.5177.

Qu, Y., Shen, W., Pei, X., Ma, F., You, S., Li, S., Wang, J., Zhou, J., 2017. Biosynthesis of gold nanoparticles by *Trichoderma* sp. WL-Go for azo dyes decolorization. J. Environ. Sci. (China) 56, 79–86. https://doi.org/10.1016/j.jes.2016.09.007.

Rahman, N.N.N.A., Shahadat, M., Won, C.A., Omar, F.M., 2014. FTIR study and bioadsorption kinetics of bioadsorbent for the analysis of metal pollutants. RSC Adv. 4, 58156–58163. https://doi.org/10.1039/c4ra05931j.

Rajendran, K., Sen, S., 2018. Adsorptive removal of carbamazepine using biosynthesized hematite nanoparticles. Environ. Nanotechnol. Monit. Manag. 9, 122–127. https://doi.org/10.1016/j.enmm.2018.01.001.

Rajendran, K., Sen, S., 2016. Optimization of process parameters for the rapid biosynthesis of hematite nanoparticles. J. Photochem. Photobiol. B Biol. 159, 82–87 https://doi.org/10.1016/j.jphotobiol.2016.03.023.

Rajput, S., Werezuk, R., Lange, R.M., Mcdermott, M.T., 2016. Fungal isolate optimized for biogenesis of silver nanoparticles with enhanced colloidal stability. Langmuir 32, 8688–8697. https://doi.org/10.1021/acs.langmuir.6b01813.

Ranjitha, V.R., Ravishankar, V.R., 2018. Extracellular synthesis of selenium nanoparticles from an *Actinomycetes Streptomyces griseoruber* and evaluation of its cytotoxicity on HT-29 cell line. Pharm. Nanotechnol. 6, 61–68. https://doi.org/10.2174/2211738505666171113141010.

Ranoszek-Soliwoda, K., Tomaszewska, E., Małek, K., Celichowski, G., Orlowski, P., Krzyzowska, M., Grobelny, J., 2019. The synthesis of monodisperse silver nanoparticles with plant extracts. Colloids Surfaces B Biointerfaces 177, 19–24 https://doi.org/10.1016/j.colsurfb.2019.01.037.

Reddy, C.V., Shim, J., Cho, M., 2017. Synthesis, structural, optical and photocatalytic properties of CdS/ZnS core/shell nanoparticles. J. Phys. Chem. Solids 103, 209–217 https://doi.org/10.1016/j.jpcs.2016.12.011.

Ren, Y.X., Dai, T.J., Luo, W.B., Liu, X.Z., 2018. Evidences of sensitization mechanism for PbSe thin films photoconductor. Vacuum 149, 190–194 https://doi.org/10.1016/j.vacuum.2017.12.017.

Reuter, S., Gupta, S.C., Chaturvedi, M.M., Aggarwal, B.B., 2011. Oxidative stress, inflammation, and cancer: how are they linked? Free Radic. Biol. Med. 49, 1603–1616. https://doi.org/10.1016/j.freeradbiomed.2010.09.006.Oxidative.

Sankapal, B.R., Ladhe, R.D., Salunkhe, D.B., Baviskar, P.K., Gupta, V., Chand, S., 2011. Room temperature chemical synthesis of highly oriented PbSe nanotubes based on negative free energy of formation. J. Alloys Compd. 509, 10066–10069 https://doi.org/10.1016/j.jallcom.2011.08.036.

Schaadt, D.M., Feng, B., Yu, E.T., 2005. Enhanced semiconductor optical absorption via surface plasmon excitation in metal nanoparticles. Appl. Phys. Lett. 86, 63106. https://doi.org/10.1063/1.1855423.

Sharma, G., Kumar, A., Sharma, S., Naushad, M., Prakash Dwivedi, R., ALOthman, Z.A., Mola, G.T., 2019. Novel development of nanoparticles to bimetallic nanoparticles and their composites: a review. J. King Saud Univ. – Sci. 31, 257–269 https://doi.org/10.1016/j.jksus.2017.06.012.

Sun, X., Gao, K., Pang, X., Yang, H., Volinsky, A.A., 2015. Thickness effect on the band gap of magnetron sputtered $Pb_{45}Se_{45}O_{10}$ thin films on Si. Phys. E Low-dimensional Syst. Nanostruct. 67, 152–158 https://doi.org/10.1016/j.physe.2014.11.021.

Syed, A., Ahmad, A., 2013. Extracellular biosynthesis of CdTe quantum dots by the fungus *Fusarium oxysporum* and their anti-bacterial activity. Spectrochim. Acta – Part A Mol. Biomol. Spectrosc. 106, 41–47. https://doi.org/10.1016/j.saa.2013.01.002.

Taourati, R., Khaddor, M., Laghzal, A., El Kasmi, A., 2020. Facile one-step synthesis of highly efficient single oxide nanoparticles for photocatalytic application. Sci. African 8. https://doi.org/10.1016/j.sciaf.2020.e00305.

Thakkar, K.N., Mhatre, S.S., Parikh, R.Y., 2010. Biological synthesis of metallic nanoparticles. Nanomed. Nanotechnol. Biol. Med. 6, 257–262 https://doi.org/10.1016/j.nano.2009.07.002.

Tugarova, A.V., Mamchenkova, P.V., Dyatlova, Y.A., Kamnev, A.A., 2018. FTIR and Raman spectroscopic studies of selenium nanoparticles synthesised by the bacterium *Azospirillum thiophilum*. Spectrochim. Acta – Part A Mol. Biomol. Spectrosc. 192, 458–463. https://doi.org/10.1016/j.saa.2017.11.050.

Vahabi, K., Mansoori, G.A., Karimi, S., 2011. Biosynthesis of silver nanoparticles by fungus *Trichoderma Reesei* (A route for large-scale production of AgNPs). Insciences J. 1, 65–79. https://doi.org/10.5640/insc.010165.

Vidhu, V.K., Philip, D., 2015. Biogenic synthesis of SnO_2 nanoparticles: evaluation of antibacterial and antioxidant activities. Spectrochim. Acta – Part A Mol. Biomol. Spectrosc. 134, 372–379. https://doi.org/10.1016/j.saa.2014.06.131.

Vyas, J., Rana, S., 2017a. Antioxidant activity and biogenic synthesis of selenium nanoparticles using the leaf extract of *Aloe Vera*. Int. J. Curr. Pharm. Res. 9.

Vyas, J., Rana, S., 2017b. Antioxidant activity and green synthesis of selenium nanoparticles using *allium sativum* extract. Int. J. Phytomedicine 9, 634. https://doi.org/10.5138/09750185.2185.

Weon, S., He, F., Choi, W., 2019. Status and challenges in photocatalytic nanotechnology for cleaning air polluted with volatile organic compounds: visible light utilization and catalyst deactivation. Environ. Sci. Nano 6, 3185–3214. https://doi.org/10.1039/c9en00891h.

Xu, T.T., Lee, J.K., 2014. Nanomaterials: electrical, magnetic, and photonic applications. JOM 66, 654. https://doi.org/10.1007/s11837-014-0923-1.

Yang, Y., Shi, J., Kawamura, G., Nogami, M., 2008. Preparation of Au–Ag, Ag–Au core–shell bimetallic nanoparticles for surface-enhanced Raman scattering. Scr. Mater. 58, 862–865 https://doi.org/10.1016/j.scriptamat.2008.01.017.

Zaleska-Medynska, A., Marchelek, M., Diak, M., Grabowska, E., 2016. Noble metal-based bimetallic nanoparticles: the effect of the structure on the optical, catalytic and photocatalytic properties. Adv. Colloid Interface Sci. 229, 80–107 https://doi.org/10.1016/j.cis.2015.12.008.

Zhu, L., Ali, A., Shu, Y., Ullah, K., Cho, K.Y., Oh, W.C., 2015. Detection of reactive oxygen species (ROS) and investigation of efficient visible-light-responsive photocatalysis via nanoscale PbSe sensitized TiO_2. Sep. Purif. Technol. 151, 184–192. https://doi.org/10.1016/j.seppur.2015.07.052.